US 20250263823A1

(19) **United States**

(12) **Patent Application Publication** (10) **Pub. No.: US 2025/0263823 A1**

Singh et al. (43) **Pub. Date: Aug. 21, 2025**

(54) **DUCTILE REFRACTORY ALLOYS WITH HIGH STRENGTH**

(71) Applicant: **Iowa State University Research Foundation, Inc.**, Ames, IA (US)

(72) Inventors: **Prashant Singh**, Ames, IA (US); **Nicolas Argibay**, Ames, IA (US); **Duane D. Johnson**, Ames, IA (US); **Hailong Huang**, Ames, IA (US); **Gaoyuan Ouyang**, Ames, IA (US)

(21) Appl. No.: **19/056,985**

(22) Filed: **Feb. 19, 2025**

Related U.S. Application Data

(60) Provisional application No. 63/555,426, filed on Feb. 20, 2024.

Publication Classification

(51) **Int. Cl.**

C22C 30/00	(2006.01)
B22D 21/00	(2006.01)
B22D 21/02	(2006.01)
C22C 27/02	(2006.01)

(52) **U.S. Cl.**

CPC ***C22C 30/00*** (2013.01); ***B22D 21/00*** (2013.01); ***B22D 21/022*** (2013.01); ***C22C 27/02*** (2013.01)

(57) **ABSTRACT**

Alloy castings are provided and comprise Nb, Ta, V, Ti, and optional Hf in controlled proportions to impart unprecedented and unexpected high ductility in refractory based alloys. Certain alloys are extremely ductile (able to sustain >50% cold roll reduction without fracture) while have high hardness (about 400HV). The combination of high thermodynamic phase stability, low-temperature ductility, and strength at room temperature makes the disclosed alloy family likely candidates as next-generation high temperature structural alloys.

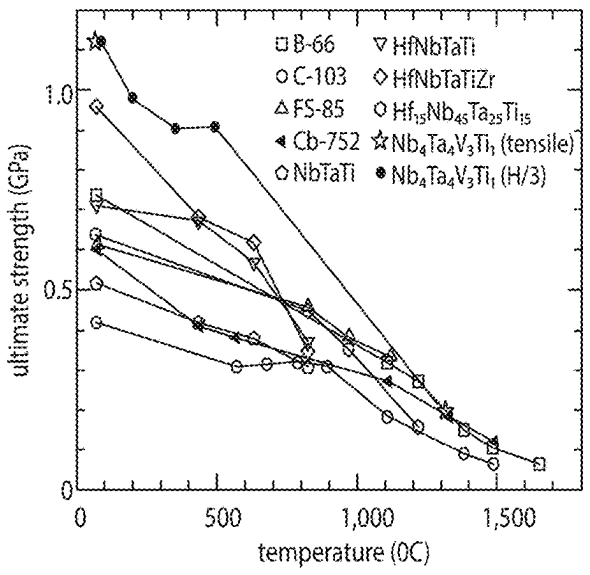

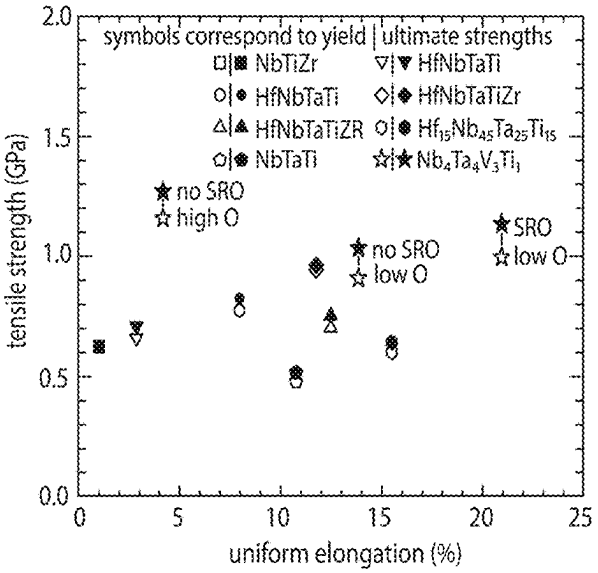

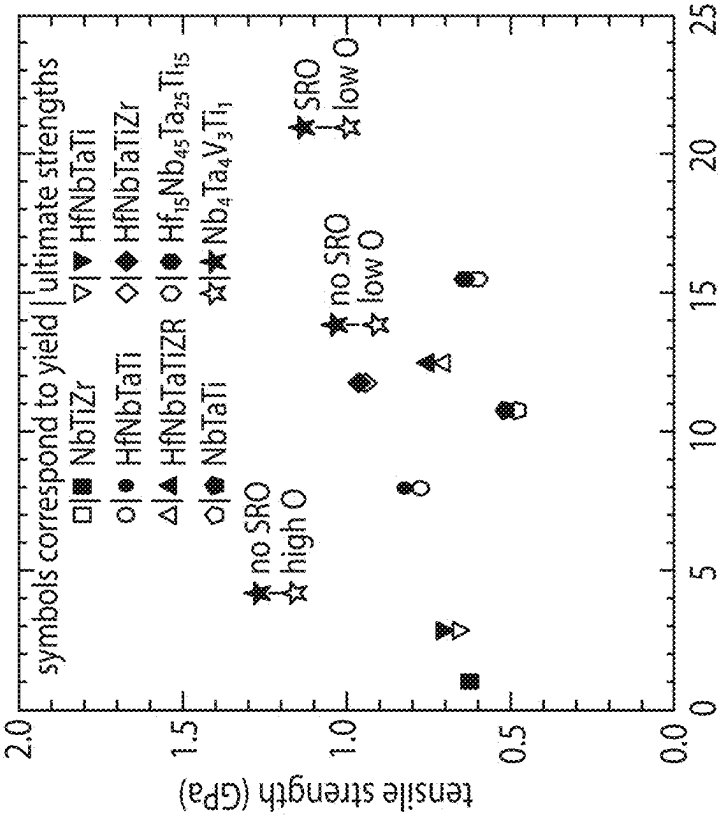
symbols correspond to yield | ultimate strengths
NbTiZr
HfNbTaTi
HfNbTaTi
HfNbTaTiZr
HfNbTaTiZR
$Hf_{15}Nb_{45}Ta_{25}Ti_{15}$
NbTaTi
$Nb_4Ta_4V_3Ti_1$
no SRO
high O
no SRO
low O
SRO
low O
tensile strength (GPa)
uniform elongation (%)
2.0
1.5
1.0
0.5
0.0
0
5
10
15
20
25

Fig. 1b

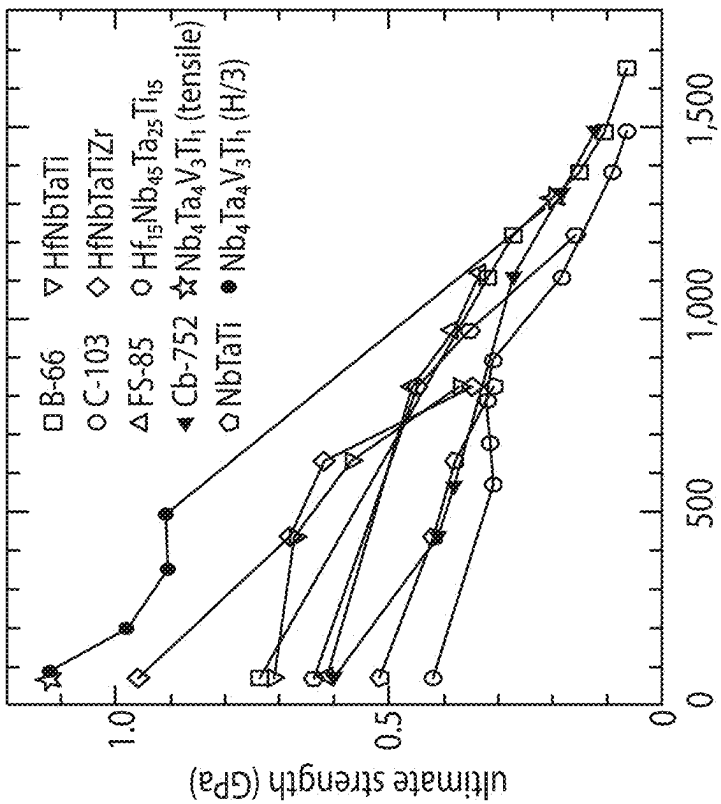
B-66
HfNbTaTi
C-103
HfNbTaTiZr
FS-85
$Hf_{15}Nb_{45}Ta_{25}Ti_{15}$
Cb-752
$Nb_4Ta_4V_3Ti_1$ (tensile)
NbTaTi
$Nb_4Ta_4V_3Ti_1$ (H/3)
ultimate strength (GPa)
temperature (0C)
1.0
0.5
0
0
500
1,000
1,500

Fig. 1a

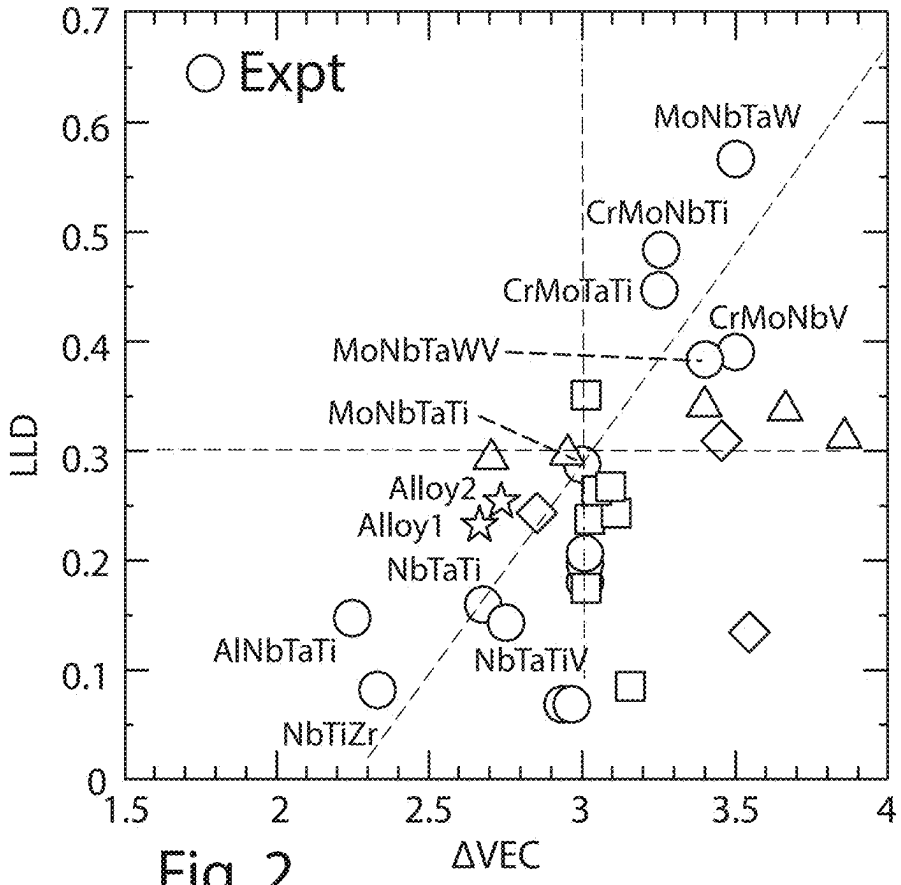

Fig. 2

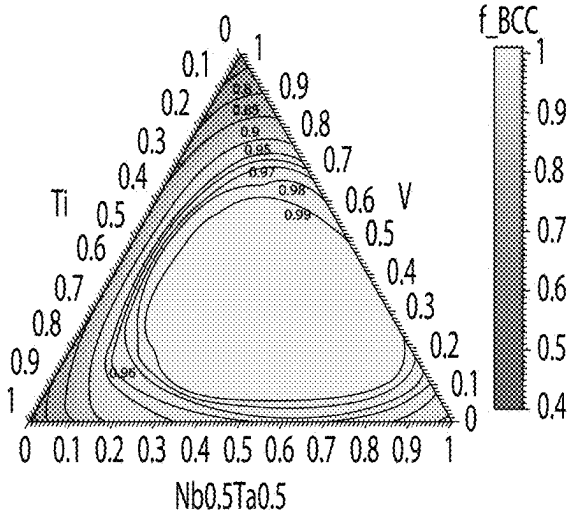

BCC phase evoluation in Nb-Ta-Ti-V MPEA

Fig. 3

Fig. 4a

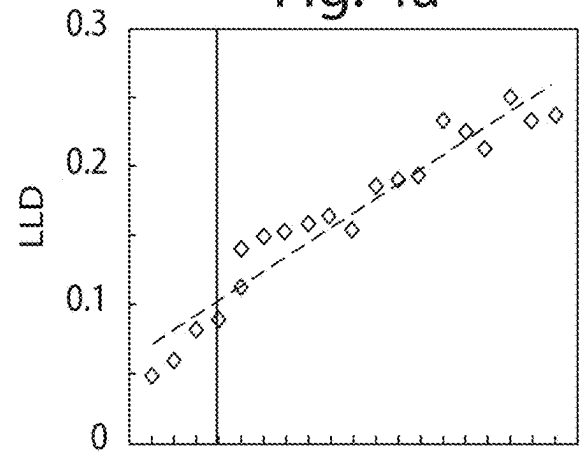

Fig. 4d

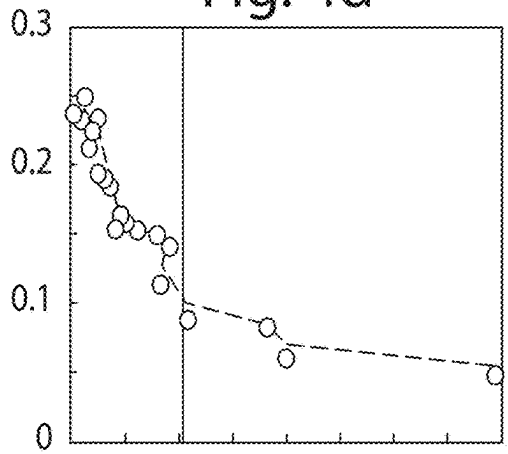

Fig. 4b

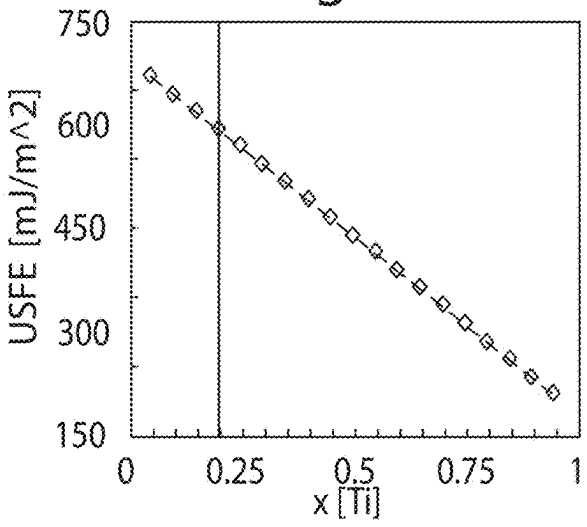

Fig. 4e

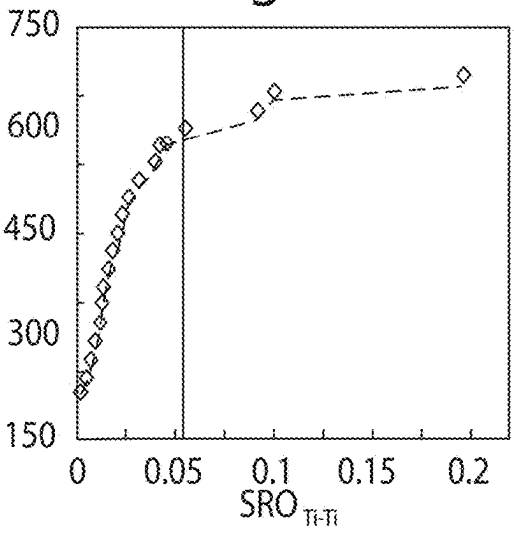

Fig. 4c

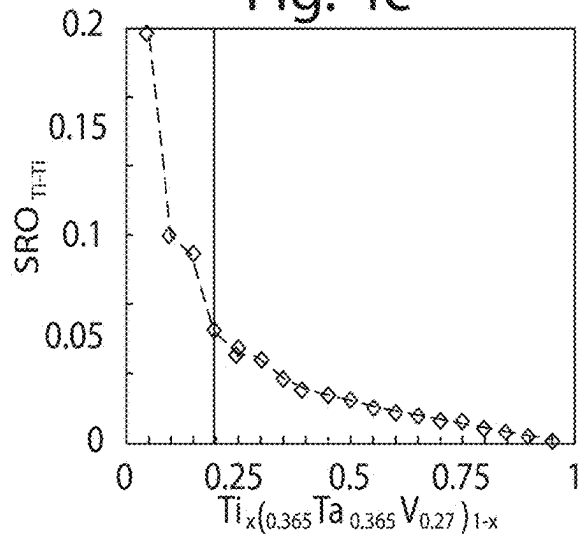

Fig. 4f

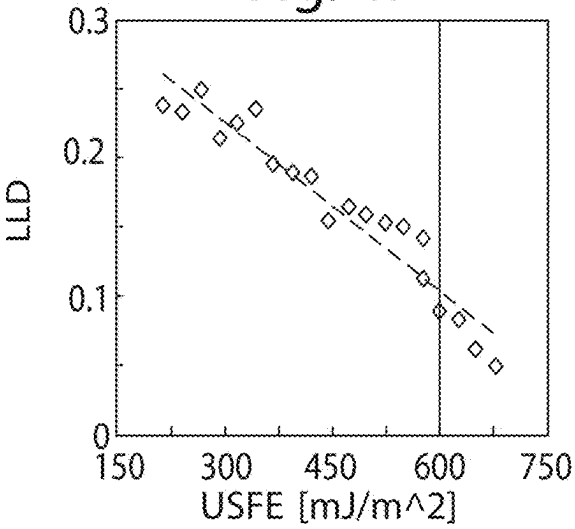

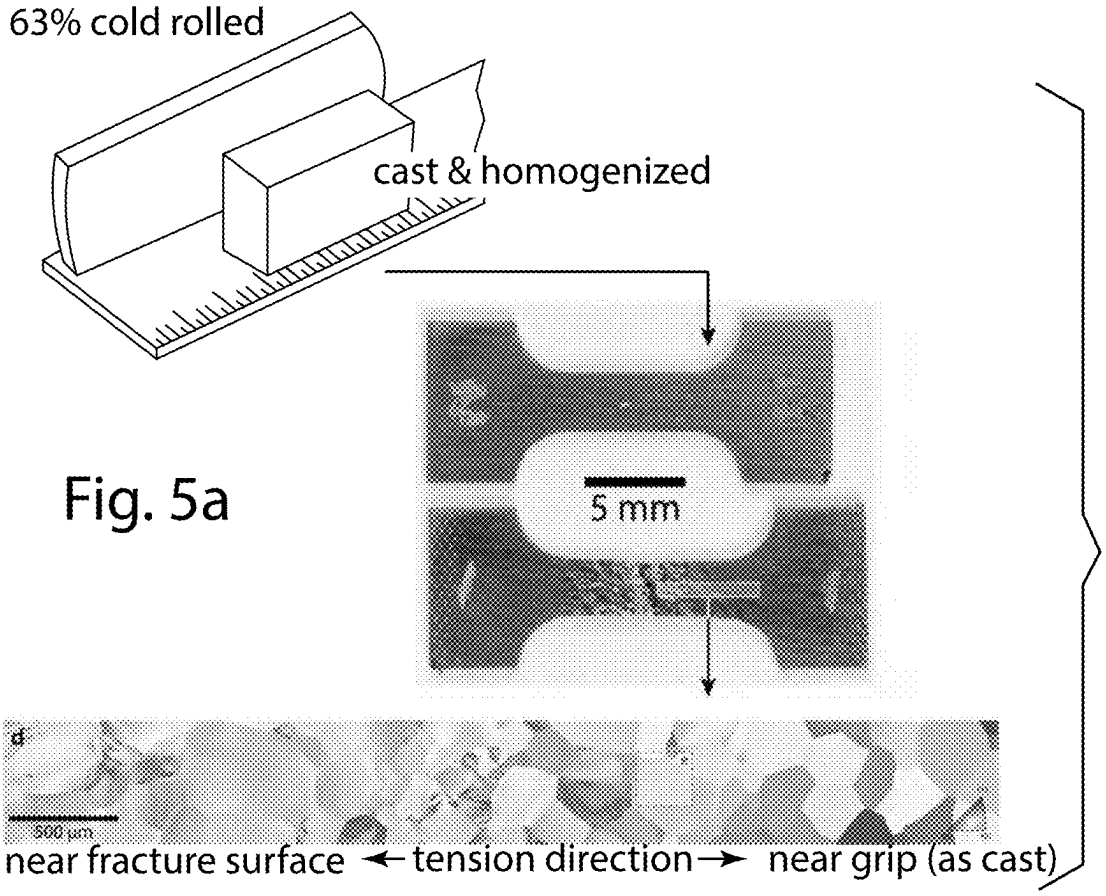
63% cold rolled
cast & homogenized
5 mm
500 µm
near fracture surface
tension direction
near grip (as cast)

Fig. 5a

Fig. 5b

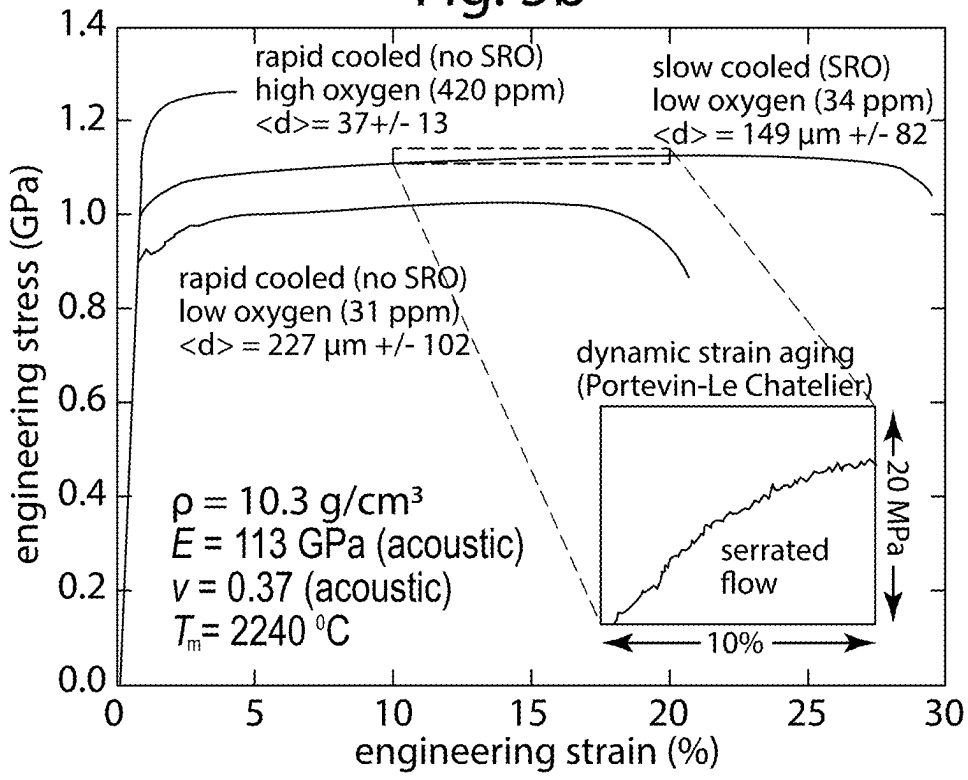
rapid cooled (no SRO)
high oxygen (420 ppm)
<d>= 37+/- 13
slow cooled (SRO)
low oxygen (34 ppm)
<d> = 149 µm +/- 82
rapid cooled (no SRO)
low oxygen (31 ppm)
<d> = 227 µm +/- 102
dynamic strain aging
(Portevin-Le Chatelier)
serrated
flow
20 MPa
10%
ρ = 10.3 g/cm³
E = 113 GPa (acoustic)
ν = 0.37 (acoustic)
Tm = 2240 °C
engineering stress (GPa)
engineering strain (%)
0.0
0.2
0.4
0.6
0.8
1.0
1.2
1.4
0
5
10
15
20
25
30

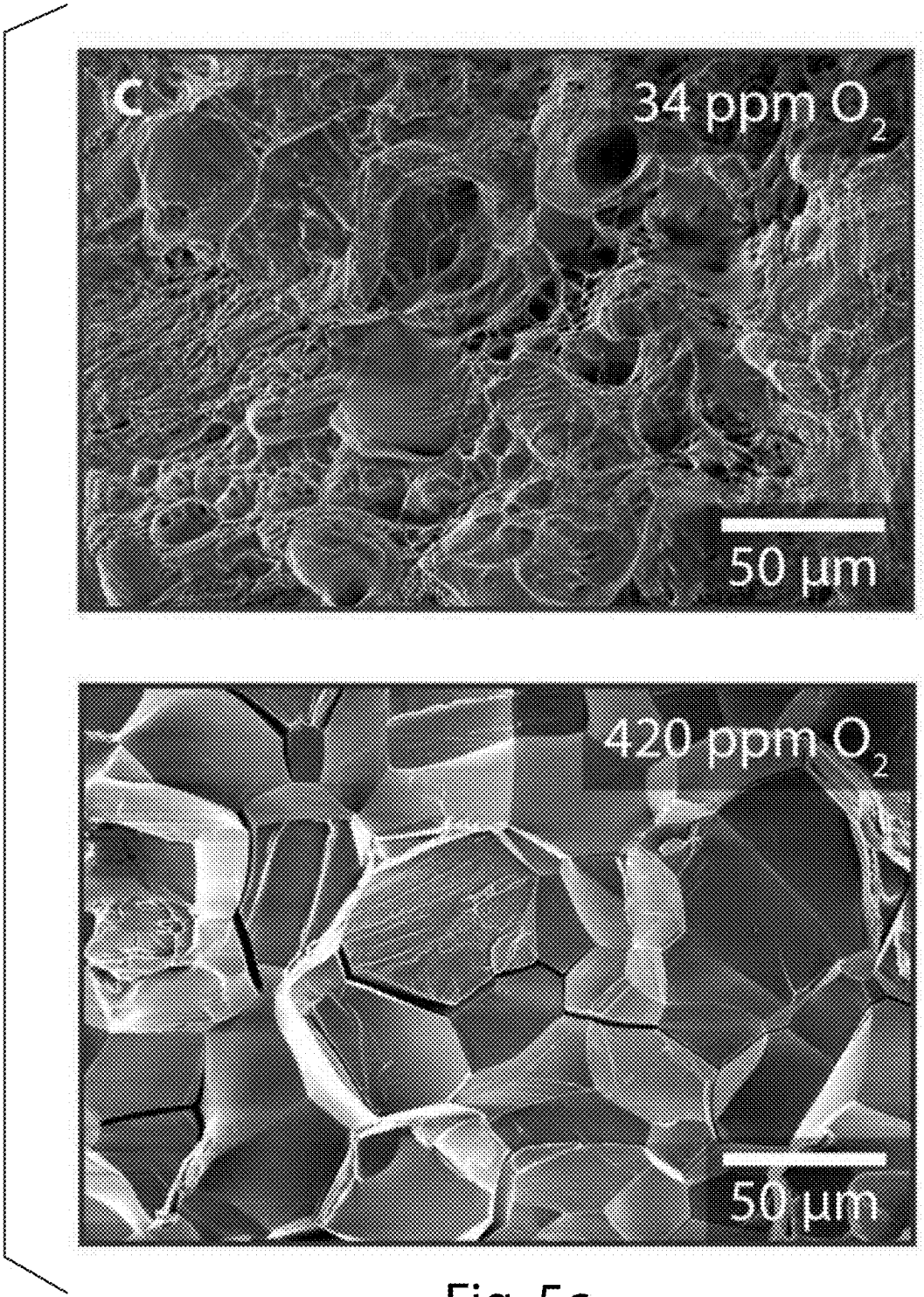

Fig. 5c

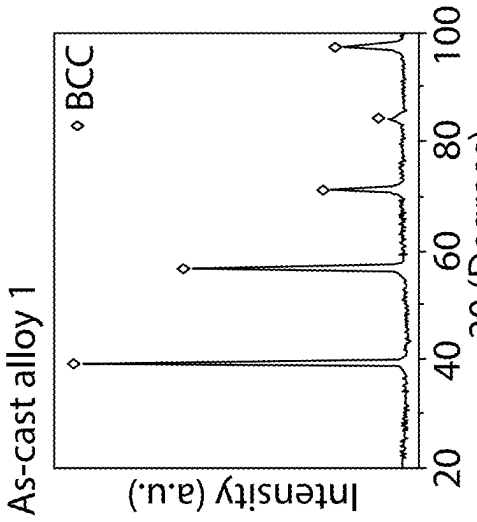

Fig. 6a

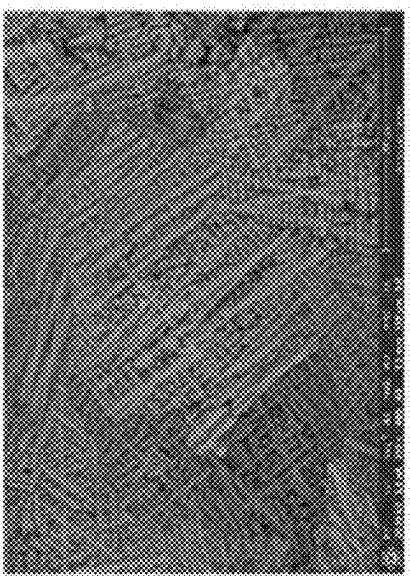

Fig. 6b

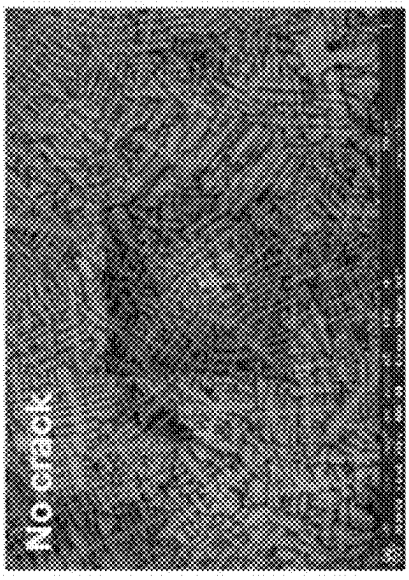

Fig. 6c

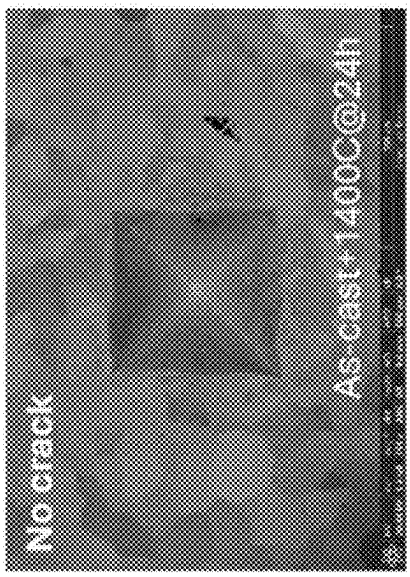

Fig. 6d

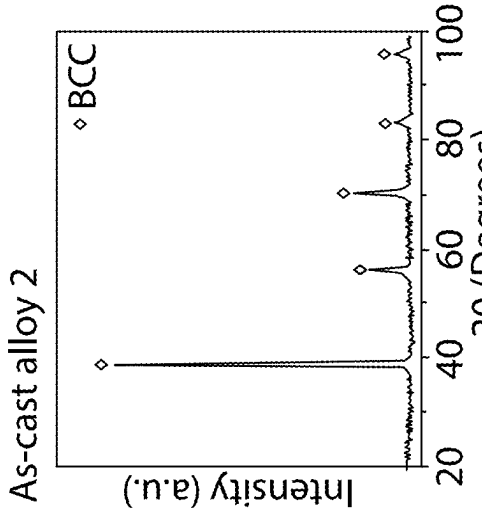

Fig. 6e

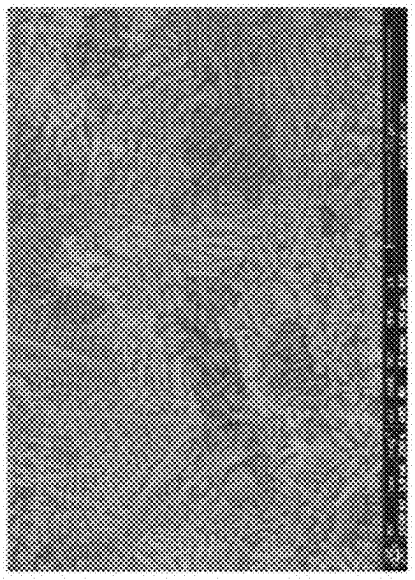

Fig. 6f

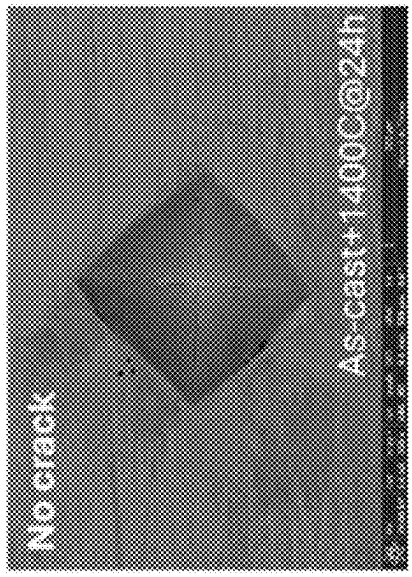

Fig. 6h

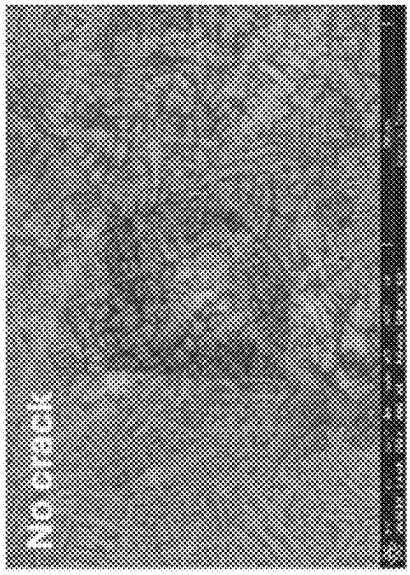

Fig. 6g

DUCTILE REFRACTORY ALLOYS WITH HIGH STRENGTH

RELATED APPLICATION

[0001] This application claims priority and benefit of provisional application Ser. No. 63/555,426 filed Feb. 20, 2024, the entire disclosure and drawings of which are incorporated herein by reference.

CONTRACTUAL ORIGIN OF THE INVENTION

[0002] This invention was made with government support under Grant No. DE-AC-02-07CH11358 awarded by the U.S. Department of Energy. The government has certain rights in the invention.

FIELD OF THE INVENTION

[0003] Refractory-element-based Multi-Principal-Element Alloys (RMPEAs) at present lack a balance of room-temperature ductility and high strength. The present invention relates to certain RMPEA compositions that meet these criteria.

BACKGROUND OF THE INVENTION

[0004] Land-based gas turbines are expected to play a vital role as the world pursues carbon neutral power generation. Hotter turbine runs more efficiently, if the turbine operation temperature can be pushed higher without damaging the turbine blades [references 1-3]. The current generation blade materials are Ni-based superalloys with a melting temperature of about 1350° C. State-of-the-art Ni-based superalloys can be operated at temperatures up to 1100° C., but this requires thermal barrier coatings and internal cooling channels to enable operation with working gas temperatures as high as 1600° C. New structural alloys that can operate at 1300° C. or higher enable significant increases in turbine efficiency, as high as 7% based on an analysis by DOE ARPA-E. Additionally, the same RMPEAs can be used to prolong the life of stamping dies for a wide range of materials forming (e.g., automobile panels), where capital costs of tooling are a key limiting factor.

[0005] RMPEAs are promising alloys for high-temperature applications. They are being developed based on high-entropy alloy (HEA) concept which presupposes that higher configurational entropy leads to higher stability and strength. Ideally, RMPEAs are single-phase material systems with potentially excellent phase stability, extremely high melting temperatures, and high specific strength via solid solution strengthening at temperatures well above 1000° C. The first two RMPEAs reported exhibiting excellent high-temperature strength are equiatomic compounds of MoNbTaW and MoNbTaVW (see references 4-6). They offer exceptional compressive yield strength of 400-700 MPa at 1600° C., whereas for a typical Ni-based superalloy, e.g. Inconel 718, the yield strength drops to near zero at about 1200° C. Such dramatic difference in mechanical strength at high temperatures underscores RMPEAs' potential. Unfortunately, these two RMPEAs are brittle at room temperature. Nor can they be manufactured using common metallurgical processes.

[0006] Considerable efforts were made to improve the ductility of many RMPEA's with limited success. In those cases where ductility was observed, the concomitant strength reduction was problematic enough to make them of limited practical utility compared to dilute refractory-based alloys like Alloy C103.

[0007] The present invention relates to RMPEA's that address the lack of balance of room-temperature ductility and high-temperature strength of the existing alloys. More particularly, the present invention relates to certain compositions and properties of RMPEAs that comprise Nb—Ta-rich RMPEAs that exhibit a combination of good room-temperature ductility for processability and thermal-cycle survivability and high-temperature strength for operating under load under extended harsh-service condition (e.g., turbine blades in gas turbines).

SUMMARY OF THE INVENTION

[0008] Embodiments of the present invention provide RMPEAs having certain compositions that exhibit a combination of good room-temperature ductility for processability. For purposes of illustration, the refractory multi-principal-element alloys (RMPEAs) pursuant to embodiments of the invention are cast or consolidated from alloy particles thereof to provide structural (load-bearing) components that have high melting temperatures, good (tensile) yield stress.

[0009] Certain embodiments of the present invention provide RMPEA alloy casting compositions which comprise Nb, Ta, V, Ti, and optional Hf in controlled proportions to impart unprecedented and unexpected high ductility and other mechanical properties to the alloy casting.

[0010] Various embodiments of the present invention provide castable RMPEA materials for higher temperature operation for, e.g., land-based gas turbine or rocket engine structural components including at least one of a combustor component, a high pressure turbine component, a low pressure turbine component, and exit nozzle component; manufacturing dies or molds; and machine or vehicle components designed to operate at elevated temperatures to allow higher strength at high temperatures, longer lifetime, and lower replacements costs, as well as improved consistency in properties and reduced failure rate. These materials and structural components can enable significant reductions in greenhouse gas (GHG) emissions, reducing the carbon footprint for electricity generation and manufacturing by enabling more efficient and longer lasting parts (i.e., reduced maintenance costs), e.g., in turbomachinery, bearings, and shaping dies, as well as addressing materials challenges to produce small-modular fission reactors and enabling plasma containment needed in planned fusion reactors.

BRIEF DESCRIPTION OF THE DRAWINGS

[0011] FIGS. **1***a* and **1***b* are Ashby-type plots for all refractory MPEAs for which there is both high-temperature strength data and room-temperature tensile ductility >10% available in literature for a comparison to Alloy 1 (Nb4Ta4V3Ti)) pursuant to a certain embodiment of the present invention wherein Nb4Ta4V3Ti (H/3) represents Vickers hardness of alloy 1 divided by 3, Tabor constant, which enables direct comparison between Vickers hardness values of alloy 1 and uniaxial strength thereof and Nb4Ta4V3Ti1 (tensile) represents uniaxial tensile values of alloy 1 obtained from tensile testing. In FIG. **1***b*, uniform elongation on the horizontal axis refers to the portion of total plastic strain that is non-localized before necking of the sample begins, e.g. see FIG. **5***b* showing engineering stress-

engineering strain behavior where the uniform elongation is from the yield point (0.2% strain offset, approximately) to the strain where the highest stress is achieved and where necking begins. Total plastic strain is uniform elongation plus non-uniform elongation. In FIGS. **1***a* and **1***b*, Alloy B-66 is Nb-5% Mo-5% V-1% Zr; Alloy C-103 is Nb-10% Hf-1% Ti-0.7% Zr; Alloy FS-85 is Nb-28% Ta-10% W-1% Zr; and Alloy Cb-752 is Nb-10% W-2.5% Zr where % are weight %.

[0012] FIG. **2** shows LLD (local-lattice distortion) plotted with respected valence electron count (VEC) for various alloys. Alloy 1 and 2 (designated by star symbols) fall in the boxed-in region (lower left quadrant), smaller LLD indicates improved room-temperature ductility of these alloys. The LLD and VEC range for which an alloy will be ductile are given by the boxed-in region are for LLD range {0 to 0.3} and VEC range {0 to 3}. Higher LLD (>0.3) and VEC (>3) reflects brittleness (reference 7). Notably, alloy 2 exhibits higher LLD and IEC compared to alloy 1, indicating superior mechanical properties. Open circles represent comparison alloys from literature, while other symbols (triangles, squares, diamonds) represent theoretical predictions for alloys of other compositions.

[0013] FIG. **3** shows a pseudo-ternary diagram showing phase stability (FCC vs BCC) as a function of composition obtained from density functional theory calculations. The equimolar Nb—Ta ratio is shown to produce the largest region of high single-phase BCC stability (i.e., the largest plateau in composition space), with largest phase fraction (f-BCC).

[0014] FIGS. **4***a*-**4***f* include plots that offer clearer outline into the alloy down-selection process by highlighting key structure-property relationships, aiding in the identification of compositions with optimal strength and ductility. FIG. **4***a* shows that LLD increases with Ti content, from 0.1 to 0.2, indicating a decrease in ductility as Ti content increases. FIG. **4***b* illustrates Unstable Stacking Fault Energy (USFE), which decreases as global Ti content increases, from 600 to 350 mJ/m^2, suggesting lower strength at higher Ti concentrations, as lower USFE typically corresponds to reduced resistance to deformation. FIG. **4***c* presents data that indicates that Ti—Ti near-neighbor Short-Range Order (SRO) parameter decreases significantly with increasing Ti content, dropping from 0.15 to below 0.05. This reduction in SRO may have implications for the material's strength and ductility, as it can affect dislocation motion and phase stability. FIG. **4***d* shows a positive correlation between LLD and Ti—Ti SRO, with LLD increasing from 0.1 to 0.3 as SRO increases. As higher LLD is associated with reduced ductile, this trend aligns with the inverse relationship between LLD and ductility in the alloy. FIG. **4***e* shows USFE plotted against Ti—Ti SRO (positive value indicated clustering), indicating that USFE increases from 350 to 750 mJ/m^2 as Ti—Ti SRO increases. This behavior suggests that greater SRO (to a point) enhances strength, consistent strengthen effect observed in ordered structures. FIG. **4***f* illustrates the inverse relationship between LLD and USFE, where a rise in USFE corresponds to a lowering of LLD. Specifically, as USFE increases from 150 to 750 mJ/m^2, LLD decreases from 0.2 to 0.1, indicating that alloys with higher USFE and lower LLD are likely to exhibit higher strength and ductility. For FIG. **4***a*, the horizontal axis is x[Ti], for FIG. **4***d*, the vertical axis is LLD and the horizontal axis is $SRO_{Ti—Ti}$, and for FIG. **4***e* the vertical axis is USFE [mJ/m^2].

[0015] FIG. **5***a* shows line drawings taken from photographs of castings of alloy 1 before and after cold-rolling and wire electrical discharge machined tensile bars before and after testing as well as EBSD (electron backscatter diffraction) mapping along the tensile bar fracture surface. FIG. **5***b* shows room-temperature tensile data showing the effects of chemical short-range ordering (SRO) and interstitial oxygen (also see FIG. **1***b*). FIG. **5***c* shows representative SEM images of fracture surfaces for low and high interstitial oxygen contents.

[0016] FIG. **6***a*, **6***e* are XRD patterns and FIGS. **6***b*, **6***f* are SEM's that demonstrate as-cast (dendritic BCC) microstructure for as-cast, furnace-cooled alloy 1 and alloy 2, respectively, before homogenization anneal. FIGS. **6***c*, **6***g* are SEM's for alloy 1 and 2, respectively, show no evidence of cracking after macroscale, room-temperature, Vickers tip (100 N) indentation. FIGS. **6***d*, **6***h* for alloy 1 and alloy 2, respectively, show no cracks in measured by Vickers tip (100 N) after 1400° C.@24 hours homogenization anneal.

DESCRIPTION OF THE INVENTION

[0017] RMPEA compositions pursuant to embodiments of the present invention were developed using a screening strategy involving high-throughput density functional theory (DFT) calculations (see reference 8 incorporated herein by reference) that provide quantitative estimates of properties, such as relative phase stability and mechanical properties. A more robust ductility specifier was developed (see reference 7 incorporated herein by reference) to address the existing challenge in designing ductile refractory alloys. This robust ductility specifier developed approach utilizes local atomic movement due to change in atomic charge correlation, i.e., local lattice distortion (LLD).

[0018] FIG. **2** illustrates that alloy 1 and alloy 2 fall in the boxed-in lower left quadrant region confirming ductility properties of these alloys. The boxed-in region [range LLD (≤0.3) and VEC (≤3)] shows the LLD and VEC range for which any alloy should be ductile. Notably, alloy 2 exhibits higher LLD and IEC compared to alloy 1. This indicates superior mechanical properties of alloy 2.

[0019] FIG. **3** shows a pseudo-ternary diagram showing phase stability (FCC vs BCC) as a function of composition and indicates that the equimolar Nb—Ta ratio produces the largest region of high single-phase BCC (body-centered cubic) stability (i.e., the largest plateau in composition space), with largest phase fraction (f-BCC).

[0020] Exhaustive density functional theory (DFT) calculations and results (FIGS. **4***a*-**4***f*) were backed by bulk-alloy synthesis and characterization at high temperatures. The combined DFT and experimental strategy led to the discovery of a critical range of Nb—Ta—V-rich MPEAs casting compositions pursuant to embodiments of the present invention that yield cast or consolidated structural (load bearing) members with unprecedented and unexpected ductility compared to any other refractory-based superalloy.

[0021] Certain alloy embodiments of the present invention are extremely ductile (able to sustain >50% cold roll reduction in thickness without fracture, (see FIG. **5***a*), while having high tensile strength (about 1.0 GPa yield), FIG. **5***b*; tensile ductility (total plastic strain which is a measure of ductility)>10%, FIG. **5***b*; and hardness (about 3.5 GPa, Table 4) all at room temperature. Also, an alloy having a high fracture toughness >30 $MPa/m^{1/2}$ Is provided.

[0022] Illustrative embodiments of the present invention provide RMPEAs having casting alloy compositions represented as follows:

TABLE 1

Casting alloy composition nominal ranges (Nb, Ta, V, Ti and optional Hf concentrations are given in atomic percent):

	Nb	Ta	V	Ti
Min.	25	0.9	0.9	0.9
Max.	45	45	33	15

	Nb	Ta	V	Ti	Hf
Min.	25	0.9	0.9	0.9	0.9
Max.	45	45	33	15	15

[0023] Two exemplar alloy compositions (in atomic %, below) were cast and discovered to exhibit high as-cast ductility, demonstrating the properties achieved by practice of certain embodiments in this invention (see Table 2):

TABLE 2

Exemplar alloy compositions that were cast and their mechanical properties and microstructures characterized; nominal (intended] compositions in atomic percent (at %).

	Nb	Ta	V	Ti	Hf
Alloy 1	33.33	33.33	25	8.33	0
Alloy 2	25	25	25	12.5	12.5

[0024] Experimental details: These alloy compositions were prepared by vacuum arc melting of pure elemental ingots on a water-cooled copper hearth with five cycles of flipping and remelting the alloy ingot to achieve higher compositional uniformity followed by solidification and slow furnace cooling. Actual measured compositions were $Nb_{32.5}$ $Ta_{35.1}V_{24.3}$ $Ti_{8.1}$ and $Nb_{25.1}$ $Ta_{25.3}V_{24.6}$ $Ti_{12.6}Hf_{12.4}$ for alloy 1 and alloy 2, respectively. Cylinders (3 mm in diameter by 5.1 mm in length) and dog-bone-shaped samples with gauge section of 6 mm (length)×3 mm (width)×0.5 mm (thickness) were electrical discharge machined (EDM) from the arc-melted, furnace-cooled chill-castings for room-temperature compressive and tensile tests, respectively. As-cast samples exhibited a two-phase polycrystalline body-centered cubic (BCC) dendritic structure, FIG. **6***a*, **6***b*. The observed dendritic structure results from heterogeneous segregation during solidification; i.e., a non-equilibrium condition, wherein dendrites are enriched in heavier atoms while the inter-dendritic regions show depletion of the same. As-cast alloy density typically is less than 11 g/cm^3.

[0025] Complete homogenization was achieved by a post-casting vacuum annealing step at 1400° C. for 24 hours, FIGS. **6***d*, **6***h*, resulting in a single-phase BCC microstructure. Embodiments of the present invention envision optionally subjecting the alloy casting to a hot isostatic pressing or other pressing steps at suitable temperature/time/pressure parameters to increase casting density and homogeneity.

[0026] In view of paragraphs 23-25 above, certain embodiments of the invention envision an alloy having a composition of 32.5% Nb, 35.1% Ta, 24.3% V, 8.1% Ti, in atomic %, having the BCC phase microstructure and room-temperature ductility, such as for example room-temperature ductility (total plastic strain) greater than 10%, or variants of that composition where the content of one or more of Nb, Ta, V, and/or Ti is/are so varied as to provide a BCC phase microstructure and room-temperature ductility, such as for example room-temperature ductility (total plastic strain) greater than 10%. Certain other embodiments envision an alloy having a composition of 25.1% Nb, 25.3% Ta, 24.6% V, 12.6% Ti, 12.4% Hf, in atomic %, having the BCC phase microstructure and room-temperature ductility, such as for example room-temperature ductility (total plastic strain) greater than 10%, or variants of that composition where the content of one or more of Nb, Ta, V, Ti and/or Hf is/are so varied as to provide a BCC phase microstructure and room-temperature ductility, such as for example room-temperature ductility (total plastic strain) greater than 10%.

[0027] Referring to FIG. **5***b*, the effect of Short-Range Order (SRO) and interstitial oxygen content on mechanical (tensile) strength are summarized for alloy 1. Slow vacuum cooling yielded some short-range ordering (SRO) and a low oxygen content of 34 ppm (atomic basis) producing a combination of high engineering strength and high engineering ductility at room temperature. This method embodiment involving slow cooling (cooling rate of ~1-10 K/s) and low oxygen content (34 ppm) was achieved by slow furnace cooling (power of) of the vacuum arc-melted casting and the latter by placing the casting on a bed of Y (yttrium) oxygen getter granular media during annealing. In FIG. **5***b*, <d> is average grain diameter.

[0028] Rapid cooling with no SRO and low interstitial oxygen content of 31 ppm produced a useful combination of high engineering strength and high engineering ductility. The rapid cooling (cooling rate of ~10,000 K/s) and low oxygen content (37 ppm) were achieved using the same vacuum furnace melting procedure as above, but instead of passive furnace cooling, the sample was placed in an oil bath to rapidly cool it.

[0029] Rapid cooling with no SRO and high interstitial oxygen content of 420 ppm produced high engineering strength with much reduced ductility. Rapid cooling (cooling rate of ~10,000 K/s) and high oxygen content (420 ppm) were achieved, this time by utilizing an oil bath quench and omitting the bed of Y granular media.

[0030] Applicant notes that chemical short range order (SRO) results in compositional deviations from the fully random distribution of alloying elements in the crystal lattice. That is, small atom clusters (with 1-2 nm diameter) form within the uninterrupted crystal lattice, where Ti enrichment (within the alloy family described herein) occurs. This deviation occurs at low temperatures during solidification or annealing. At high enough temperatures, such as the homogenization annealing temperature; e.g., 1400 degree C., the elemental distribution becomes fully random. As temperature drops during cooling of the alloy, entropy decreases such that the alloys tend to want to form clusters with slightly enriched/deficient zones. This is a subtle effect that is difficult to measure but can have a large impact on ductility and strength due to how dislocations interact with the clusters during deformation of the alloy. Certain method embodiments of the invention envision optimizing alloy solidification cooling rate, such as for example by slow furnace cooling, to produce the effect of some clustering with low oxygen interstitial content. This

effect was experimentally confirmed by improvements in both strength and ductility of the as-cast alloy as shown in FIG. **1***b* and FIG. **5***b*.

[0031] Notably, the rapidly cooled specimen with low oxygen content (31 ppm) and no SRO clustering exhibited reduced room temperature strength and ductility as compared to the optimized processing just described.

[0032] The rapidly cooled specimen with high oxygen content (420 ppm O) and no SRO clustering exhibited high strength but greatly reduced ductility indicative of a microstructure having elemental distribution that is fully randomized (in a high-entropy condition) but suffering from adverse effects of high oxygen content.

[0033] As-cast samples of alloy 1 and alloy 2 exhibited adequate room temperature ductility and yield strength at room temperature (see Table 3 and FIG. **5***b*).

TABLE 3

Listing of densities, Young's modulus, room-temperature (RT) compressive and tensile properties for alloy 1 and alloy 2.

Sample	Type of Mechanical tests	Density g/cc	0.2% Yield strength MPa	Specific 0.2% Yield strength MPa · cc/g	Young's modulus GPa	Total strain %
Alloy 1	Compressive	10.44	961	92	127	>50
	Tensile		1025	98		26
Alloy 2	Compressive	10.30	1163	113	113	>50

[0034] With respect to the mechanical testing of Table 3, FIG. **5***a* (top portion) illustrates that alloy 1 exhibited room-temperature ductility exceeding 50% by cold-rolling with multiple thickness reductions in 3% steps wherein no evidence of cracking was observed. FIG. **5***b* presents a comparison of alloy 1 before and after the tensile test exhibiting 26% ductility (total plastic strain) in the tension test. Total plastic strain is a measure of ductility (i.e. unrecoverable deformation, so does not include elastic strain which is fully reversible).

[0035] Moreover, EBSD mapping along the tensile bar fracture surface, and SEM electron channeling contrast images highlighting key deformation features near the midpoint of the EBSD map indicated that, in the region bounded by the dotted lines of FIG. **5***b*, slip bands, nanoscale deformation twins, and dislocation forests were observed.

[0036] FIGS. **1***a* and **1***b* show Ashby-type plots for all refractory MPEAs for which there is both high-temperature strength data and room-temperature tensile ductility >10% available in literature for a comparison to test data from Alloy 1 (Nb4Ta4V3Ti)) pursuant to certain embodiments of the present invention at multiple temperatures.

[0037] Table 4 below shows Vickers hardness of as-cast, post 50% cold worked (CW rolling) with and without subsequent 1300° C.@1 hour anneal, and after an additional 1400° C.@24 hours homogenization anneal.

[0038] Also, interferometer topographical maps of hardness indentation test impressions for alloy 1 and alloy 2 were made and also showed no evidence of cracks typically associated with brittle deformation. FIGS. **6***c*, **6***d*, **6***g*, and **6***h* are SEMs showing hardness indentations with no evidence of cracking.

TABLE 4

Sample	Processing condition	Hardness (GPa)
Alloy 1	as chill-cast	3.43 ± 0.01
	As cast + 50% CW	4.10 ± 0.07
	As cast + 50% CW + 1300 C. @1 h	3.62 ± 0.06
	As cast + 1400 C. @24 h	4.45 ± 0.08
Alloy 2	as chill-cast	3.68 ± 0.06
	As cast + 50% CW	4.69 ± 0.20
	As cast + 50% CW + 1300 C. @1 h	4.10 ± 0.16
	As cast + 1400 C. @24 h	4.29 ± 0.13

[0039] Although certain embodiments of the invention have been described in detail above, those skilled in the art will appreciate that changes and modifications can be made therein without departing from the scope of the invention as set forth in the appended claims.

REFERENCES, WHICH ARE INCORPORATED HEREIN BY REFERENCE

[0040] 1 P. Caron, High y' solvus new generation nickel-based superalloys for single crystal turbine blade applications, Superalloys 2000 (2000) 737-746.

[0041] 2 R Darolia, Development of strong, oxidation and corrosion resistant nickel-based superalloys: critical review of challenges, progress and prospects, international materials reviews 64(6) (2019) 355-380.

[0042] 3 U.S. Department of Energy Advanced Research Projects Agency-Energy (ARPA-E), Funding Opportunity No. DE-FOA-0002337, Ultrahigh Temperature Impervious Materials Advancing Turbine Efficiency (Ultimate) (2020)

[0043] 4 D. B. Miracle, O. N. Senkov, A critical review of high entropy alloys and related concepts, Acta materialia 122 (2017) 448-511.

[0044] 5 O. N. Senkov, G. B. Wilks, D. B. Miracle, C. P. Chuang, P. K. Liaw, Refractory high-entropy alloys, Intermetallics 18(9) (2010) 1758-1765.

[0045] 6 O. N. Senkov, G. B. Wilks, J. M. Scott, D. B. Miracle, Mechanical properties of $Nb_{25}Mo_{25}$ $Ta_{25}W_{25}$ and $V_{20}Nb_{20}MO_{20}Ta_{20}W_{20}$ refractory high entropy alloys, Intermetallics 19(5) (2011) 698-706.

[0046] 7 P Singh, B Vella, G Ouyang, N Argibay, J Cui, R Arroyave, D D Johnson, A ductility metric for refractory-based multi-principal element alloys, Acta Materialia 257, 1-15 (09-15-2023).

[0047] 8 D D Johnson, P Singh, A V Smirnov, N Argibay, Universal maximum strength of solid metals and alloys, Physical Review Letters 130, 166101 (2023).

We claim:

1. A ductile RMPEA alloy having a composition comprising Nb, Ta, V, Ti, and optional Hf in controlled proportions to impart high ductility to the alloy at room temperature.

2. The alloy of claim **1** having such high ductility that the alloy is able to sustain >50% cold roll reduction in thickness without fracture.

3. The alloy of claim **1** having a minimum room-temperature ductility (total plastic strain)>10%.

4. The alloy of claim **3** having a high fracture toughness >30 $MPa/m^{1/2}$.

5. The alloy of claim **4** having a room-temperature hardness >3.0 GPa.

6. The alloy of claim **5** having a room-temperature uniaxial tensile strength >1.0 GPa.

7. An alloy having a composition, in atomic percent (%): 25 to 45% Nb, 0.9 to 45% Ta, 0.9 to 33% V, and 0.9 to 15% Ti.

8. An alloy having a composition, in atomic percent (%): 25 to 45% Nb, 0.9 to 45% Ta, 0.9 to 33% V, 0.9 to 15% Ti, and 0.9 to 15% Hf.

9. An alloy having a composition of 32.5% Nb, 35.1% Ta, 24.3% V, 8.1% Ti, in atomic %, or variants of that composition where the content of one or more of Nb, Ta, V, and/or Ti is/are so varied as to provide a BCC phase microstructure.

10. An alloy having a composition of 25.1% Nb, 25.3% Ta, 24.6% V, 12.6% Ti, 12.4% Hf, in atomic %, or variants of that composition where the content of one or more of Nb, Ta, V, Ti and/or Hf is/are so varied as to provide a BCC phase microstructure.

11. A solidified alloy body comprising the alloy of claim **7**.

12. The solidified body of claim **11** which is cast and annealed to provide a single BCC phase microstructure.

13. A solidified alloy body comprising the alloy of claim **8**.

14. The solidified body of claim **13** which is cast and annealed to provide a single BCC phase microstructure.

15. A method of casting, comprising providing a melt of an alloy having the composition of claim **7** and solidifying the melt in a manner to provide a BCC phase microstructure.

16. A method of casting, comprising providing a melt of an alloy having the composition of claim **8** and solidifying the melt in a manner to provide a BCC phase microstructure.

* * * * *